

# Rapid manufacturing of mechanoreceptive skins for slip detection in robotic grasping

Alexi Charalambides and Sarah Bergbreiter

Dept. of Mechanical Engineering and

Institute for Systems Research

University of Maryland, 2181 Glenn L. Martin Hall

College Park, MD 20742, USA

(acharala, sarahb)@umd.edu

August 31, 2016

## Abstract

This work demonstrates a rapid manufacturing process and taxel geometry to create the first large area, all-elastomer “robot skin” capable of 3-axis tactile sensing. The milling-based process avoids clean room time while producing features over multiple length scales, from 10s of microns to 10s of centimeters, and molds all-elastomer materials to create a mechanically flexible skin. Taxels can detect applied loads using either a contact resistive approach that uses simple circuitry, or a capacitive approach that provides high dynamic range. Using the contact resistive approach, normal force range and resolution were 8 N and 1 N, respectively, and shear force range and resolution were 450 mN and 100 mN, respectively. Using the capacitive approach, normal force range and resolution were 10 N and 100 mN, respectively, and shear force range and resolution were 1500 mN and 50 mN, respectively. A robot skin the size of a human hand was manufactured with 12 taxels, and was capable of detecting normal and shear loads over a large area. Finally, a single contact resistive taxel was integrated into a one degree-of-freedom gripper, and was able to detect and prevent slip of a grasped object.

# 1 Introduction

As the field of robotics progresses towards autonomy, advanced tactile sensors are pivotal in enabling safe and dexterous interaction between a robot and its environment [1, 2]. Robotic tasks that generally rely on vision alone, such as grasping, are greatly enhanced with the addition of tactile sensing [3]. Shear force sensing in addition to normal force sensing is especially important in detecting slip of a grasped object [4]. Other wearable systems such as exoskeletons [5], shoes [6, 7], and gloves [8, 9] also stand to benefit from affordable, sensor rich “robot skins” that provide real-time force vectors over a large area.

Over the past three decades, notable progress has been made in the field of tactile sensing. Camera-based tactile sensors, in which a soft material is pressed and the deformation is processed visually, have been able to achieve microscale spatial resolution but they’re typically limited to a small sensing area and have large, specialized hardware [10]. More compact and versatile sheets of tactile sensor arrays have also been developed [11], and leverage MEMS manufacturing to create microscale sensor geometries essential to multiaxis sensing. However, this method typically results in laborious and complicated multilayer assembly with sub newton force ranges [12]. MEMS manufacturing also limits the sensing area to that of a silicon wafer [13]. Other tactile sensors which have large sensing areas have been limited to normal force sensing only [14, 15], or have had limited flexibility [16]. Microfluidic eutectic indium gallium (eGaIn) tactile sensors have achieved remarkable flexibility but are potentially hazardous if ruptured [17]. Therefore, there is a need for a flexible, large area tactile sensor array capable of shear force sensing in addition to normal force sensing.

The transduction method also plays an important role in the design and performance of tactile sensors. Flexible tactile sensor arrays typically utilize parallel-plate style capacitors [18], or resistive serpentines or strips to detect applied loads [19]. Elastomer-based piezoresistive sensors tend to suffer from electromechanical hysteresis [20, 21] and capacitive sensors [11, 22] require significant efforts in shielding. The sensor design in this paper can support multiple transduction methods to trade off performance metrics for simplicity in integration. For example, a prosthetic sensor interface may not require the same dynamic range as a robotic manipulation application.

In this work, an all-elastomer large area robot skin capable of shear and normal force sensing was developed. A contact resistive sensing technique to

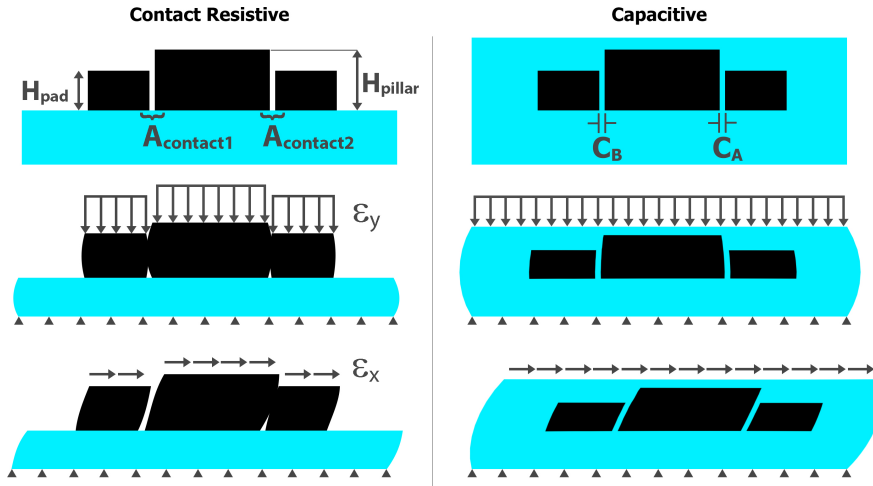


Figure 1: Cross-sectional view of the sensor architecture for the contact resistive (left) and capacitive (right) approaches. Blue areas are PDMS, and black are conductive-PDMS. [Left] As forces are applied, the “pillar” and “pads” come into physical contact and cause a measurable change in contact resistance. As a normal force is applied, the pillar and pads come into contact causing a uniform decrease in contact resistance on each side. As a shear force is applied, contact resistance decreases in the direction of shear and increases on the opposite side. [Right] An additional layer of PDMS is used to encapsulate the sensing elements for capacitive sensing [11]. As a normal force is applied, the sensor flattens and expands through Poisson’s effect causing a uniform decrease in capacitance. As a shear force is applied, capacitance increases in the direction of shear and decreases on the opposite side.

simplify electronics and minimize hysteresis was proposed and modeled using finite element analysis. Robot skins were created using a novel manufacturing process that facilitated microscale features over a large area, and produced a robot skin as large as a human hand. Force characterization was carried out for both contact resistive and capacitive sensing modalities. A single contact resistive taxel was incorporated into a one degree-of-freedom robotic gripper for slip detection and 3-axis sensing was also demonstrated on a robot skin the size of a human hand.

## 2 Taxel Architecture

Two sensing modalities are presented in this work: a *contact resistive* approach to simplify electronics and minimize electromechanical hysteresis, and a high dynamic range *capacitive* approach based on prior work [11], Fig. 1. A contact resistive sensing technique was developed in which two conductive features, referred to as the “pillar” and “pad”, come into physical contact as loads are applied. As a normal force is applied, the pillar and pads flatten and expand through Poisson’s effect, and come into contact causing a uniform decrease in contact resistance on each side. Meanwhile, a shear force results in a differential contact resistance; contact resistance decreases in the direction of shear and increases on the opposite side.

In the capacitive sensing approach, the sensor is encapsulated with a dielectric to form a capacitor between the pillar and pad. As a normal force is applied, the sensor flattens and expands through Poisson’s effect, the capacitor gap increases, and the capacitance decreases on each side uniformly. Meanwhile, a shear force results in an increase in capacitance in the direction of loading, and a decrease in capacitance on the opposite side.

Elastomers such as polydimethylsiloxane (PDMS) are especially favorable for these architectures since they are incompressible (Poissons ratio near 0.5), which maximizes lateral expansion under normal deformation. The contact resistive approach differs from previous contact resistive work [23] in that the sensor circuit is open in the unloaded state and becomes closed as forces are applied, rather than being continuously closed.

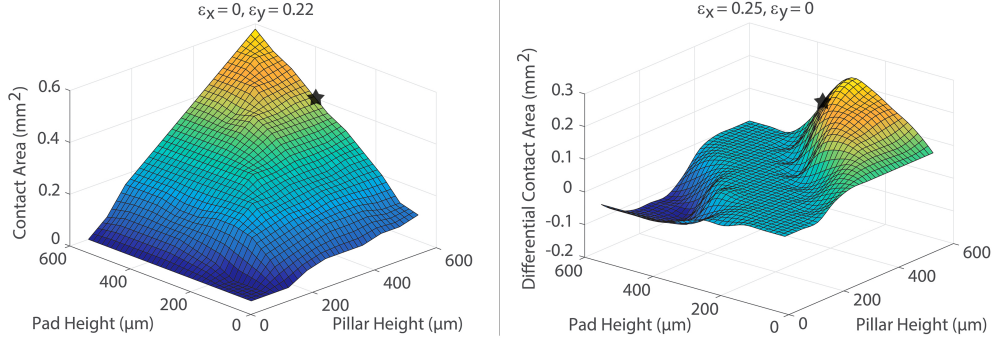


Figure 2: Parametric study of the contact resistive geometry using finite element analysis. Normal (left) or shear (right) displacements are applied, and the contact area is shown as a function of pillar and pad heights. The black star is the selected geometry. In the case of shear, differential contact area is plotted and is defined as  $A_{contact2} - A_{contact1}$ .

### 3 Finite Element Modeling

A 2D nonlinear, large deformation finite element model was written in ANSYS Mechanical APDL 14.5 to evaluate the effects of sensor geometry on contact area between the pillar and pads when subject to shear and normal deformation modes. As contact area increases the contact resistance decreases; therefore, a sensor architecture that maximizes contact area under normal deformation while maximizing differential contact area under shear deformation was desired (where differential contact area was defined as  $A_{contact2} - A_{contact1}$ , Fig. 1).

In this study, the heights of the pillar,  $H_{pillar}$ , and pads,  $H_{pad}$ , were varied from 60  $\mu\text{m}$  to 600  $\mu\text{m}$ , Fig. 2. Preliminary simulations showed that the smallest gap between the pillar and pads enabled the highest contact area. Therefore, the smallest gap that could be reliably fabricated was selected, which was 30  $\mu\text{m}$  (20  $\mu\text{m}$  and 10  $\mu\text{m}$  gaps were also producible but with lower yield). A fixed boundary condition was applied to the bottom edge in both normal and shear simulations. Normal and shear displacements were applied on top of the pillar and pads, and were proportional to the total thickness of the sensor. In essence, this created a strain-controlled boundary condition, and was an important technique in normalizing the data because the total thickness of the sensor varied between simulations. In normal simulations,

a displacement was applied that resulted in a net normal strain,  $\varepsilon_y$ , of 0.22, while in shear simulations a displacement was applied that resulted in a net shear strain,  $\varepsilon_x$ , of 0.25. A linear-elastic material model based on prior work [11] was used for the PDMS and conductive-PDMS with moduli of 1 MPa and 1.5 MPa, respectively, and both with a Poisson's ratio of 0.49.

Two competing phenomenon were observed. In normal displacement simulations, contact area increased as both the pillar and pad heights increased and was maximal when they were equal. Meanwhile in shear displacement simulations, when the heights were equal a differential contact area of zero was observed due to both pads being in contact with the pillar equally. A maximum was observed at  $H_{pillar} = 600 \mu\text{m}$  and  $H_{pad} = 300 \mu\text{m}$ . Therefore, a geometry that was selected as a compromise between normal and shear force sensing as represented by the black star:  $H_{pillar} = 600 \mu\text{m}$  and  $H_{pad} = 400 \mu\text{m}$ .

## 4 Manufacturing

Computerized numerical control (CNC) milling and micromachining has been widely used to fabricate lab-on-a-chip devices [24, 25], PDMS microstructures and adhesives [26, 27], and even pneumatic logic circuits [28]. In this work, a milling process to cast a conductive elastomer was developed to achieve microscale features over a large area, Fig. 3. This was preferred to clean room fabrication from prior work [11] due to the larger available workspace and significantly reduced time and money required for fabrication. For example, clean room work requires the outsourcing of masks for photolithography, expensive machines and chemicals, and many hours of processing time by a highly trained individual all while being limited to the working area/volume of a silicon wafer. Meanwhile, a design cycle with the developed manufacturing process takes less than 12 hours to go from concept to in-hand and ready for testing without sacrificing microscale features. Milling has the added benefit of producing highly vertical sidewalls even in tall features (greater than 400  $\mu\text{m}$ ), which is difficult to achieve with clean room techniques such as deep reactive ion etching (DRIE).

A stock of acrylic (McMaster-Carr, 8560K355) was milled in a Roland MDX-540SA desktop mill, with a workspace of approximately 12 in by 16 in, using a 406  $\mu\text{m}$  diameter endmill (Microcut USA, 82016). NC instructions were coded in Tool Path Language, and generated using CAMotics 1.0.0. No

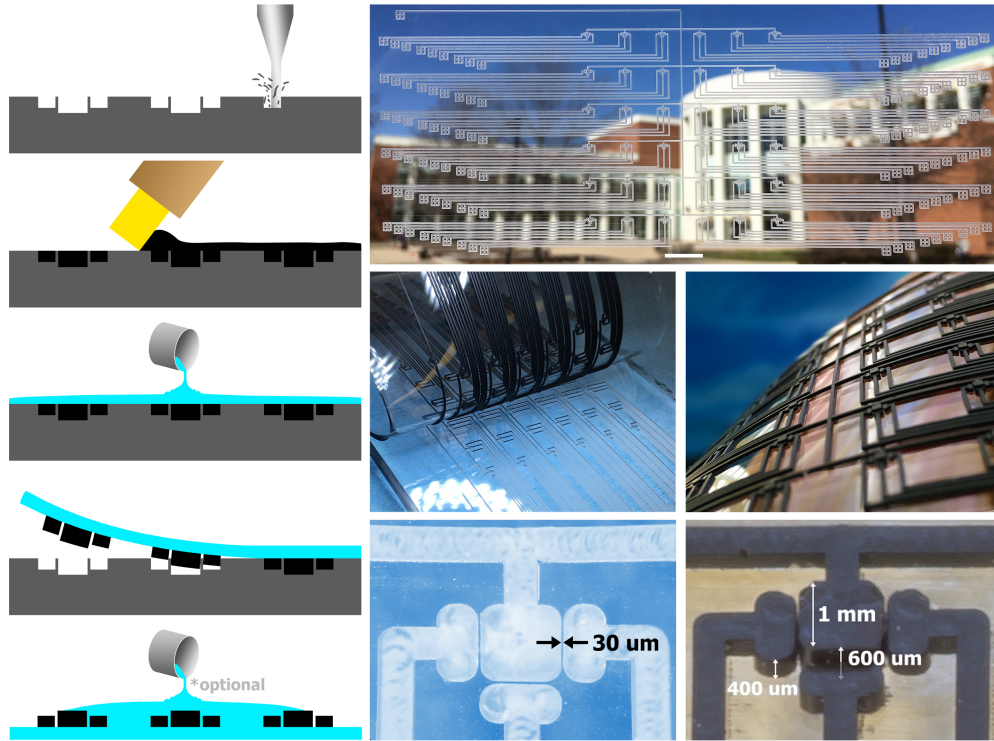


Figure 3: [Left] Manufacturing flow chart: acrylic is milled, refilled with CNT/PDMS, coated with PDMS, and peeled from mold. It can then be coated with additional PDMS to encapsulate the sensor for capacitive sensing. [Top] Acrylic mold after milling; scale bar is 1 cm. [Center] Robot skin being peeled from the mold. [Right] Isometric view of the robot skin. [Bottom] Close-up of a single taxel in the acrylic mold. [Bottom Right] Close-up of a single taxel after peeling from the mold.

rough cutting for planarizing purposes was necessary as seen in other work [28]; the stock was sufficiently planar as received. Instead, it was mounted in the CNC machine and leveled by a manual procedure: trenches of varying depths, 0  $\mu\text{m}$ , 100  $\mu\text{m}$ , 200  $\mu\text{m}$ , and 300  $\mu\text{m}$  deep, were milled in the four corners of the stock followed by minor adjustments until each corner exhibited three trenches. The stock was cut at 10 mm/min at 8000 rpm in taxel areas, and 80 mm/min at 10,000 rpm elsewhere, and finished in approximately 2-3 hours. In the presented design, this method produced features that were 400  $\mu\text{m}$  and 600  $\mu\text{m}$  deep, had a minimum size of 30  $\mu\text{m}$ , and create an array of 6 by 6 taxels spaced every 1 cm. The total area of the mold was 7 in by 4 in.

The mold was refilled with a conductive elastomer. Carbon nanotubes (CNT) (Cheap Tubes, 030103) and 10:1 PDMS (Dow Corning, Sylgard 184) were mixed at a total weight percent of 7 wt.% carbon nanotubes in a centrifugal mixer (Thinky, ARE-310) at 2000 rpm for 90 sec. CNTs were found to be favorable over spherical particles, such as carbon black and silver nanopowder, and exhibited excellent mechanical and electrical properties in PDMS with high yield. Particles such as silver nanowires were too cost prohibitive and were not explored. After mixing, the resulting tar-like CNT/PDMS composite was spread over the mold and planarized using a screen printing squeegee (Ryonet). The mold was placed in an oven at 80°C, a temperature low enough to avoid thermal warping of the acrylic (i.e., below the glass transition temperature), for 30 min to partially cure the CNT/PDMS. After allowing to cool, 10:1 PDMS was poured over the mold and placed in vacuum for 20 min to remove air bubbles, then cured in an oven at 80°C for 90 min. Lastly, the entire robot skin was peeled from the mold, which can be reused, further saving time and money. For capacitive sensing, additional PDMS is poured over the skin, vacuumed, and cured to encapsulate the taxels in a dielectric.

Each taxel consisted of one pillar and three adjacent pads, with gaps of 30  $\mu\text{m}$  between the pillar and pads. Four pads could not be accommodated due to the space requirements of the electrical routing to the pillar using the 406  $\mu\text{m}$  endmill. The total contact resistive robot skin thickness was 980  $\mu\text{m}$ , with a PDMS layer thickness of approximately 380  $\mu\text{m}$ . The completed mold and robot skin can be seen in Fig. 3.

## 5 Robot Skin Characterization

### 5.1 Test Setup

Normal and shear displacements were applied using a Thorlabs PT3-Z8 3-axis stage equipped with a 3 by 3 mm acrylic probe, and resultant forces were collected with an ATI Nano17 6-axis force/torque sensor, Fig. 4. Contact resistances were measured via an Arduino Uno and voltage divider, while capacitance was measured with an AD7745/46 evaluation board. 3-axis testing was performed on a single taxel over 5 trials for each sensing modality.

### 5.2 Normal Force

A normal force resulted in a decrease in voltage or decrease in capacitance across all 3 pads as intended, Fig. 5. In the contact resistive approach, the taxel was unresponsive below 1 N, saturated above 8 N, and had a resolution of approximately 1 N. This was because below 1 N the pillar and pads were not yet in contact, while above 8 N the sensor can compress no further. The range can be tuned by adjusting the pillar height, pad height, and gap between pillar and pads, and is still useful for robotic manipulation applications [29]. However, by using capacitive sensing the range and resolution were significantly improved, up to 10 N and 100 mN, respectively. In this case, the interstitial PDMS dielectric enables finer motion of the pillar and pads without reaching saturation. This normal force dynamic range, 100:1, was greater than prior work [11], 42:1, due to the taller pillar and pad heights enabled from the milling manufacturing process (from 300  $\mu\text{m}$  and 100  $\mu\text{m}$  to 600  $\mu\text{m}$  and 400  $\mu\text{m}$  for the pillar and pad, respectively), although the gap was slightly larger (from 20  $\mu\text{m}$  to 30  $\mu\text{m}$ ).

### 5.3 Shear Force

Shear forces were applied in the direction of each pad, Fig. 5. A small normal force of approximately 1-2 N was applied before shearing to improve contact between the acrylic probe and the taxel, while minimizing the influence of normal force on the results. A decrease in voltage was observed across the intended pad in each shear case, while the voltage of the other pads remained relatively unchanged. Shear force range and resolution were approximately 450 mN and 100 mN, respectively for the contact resistance

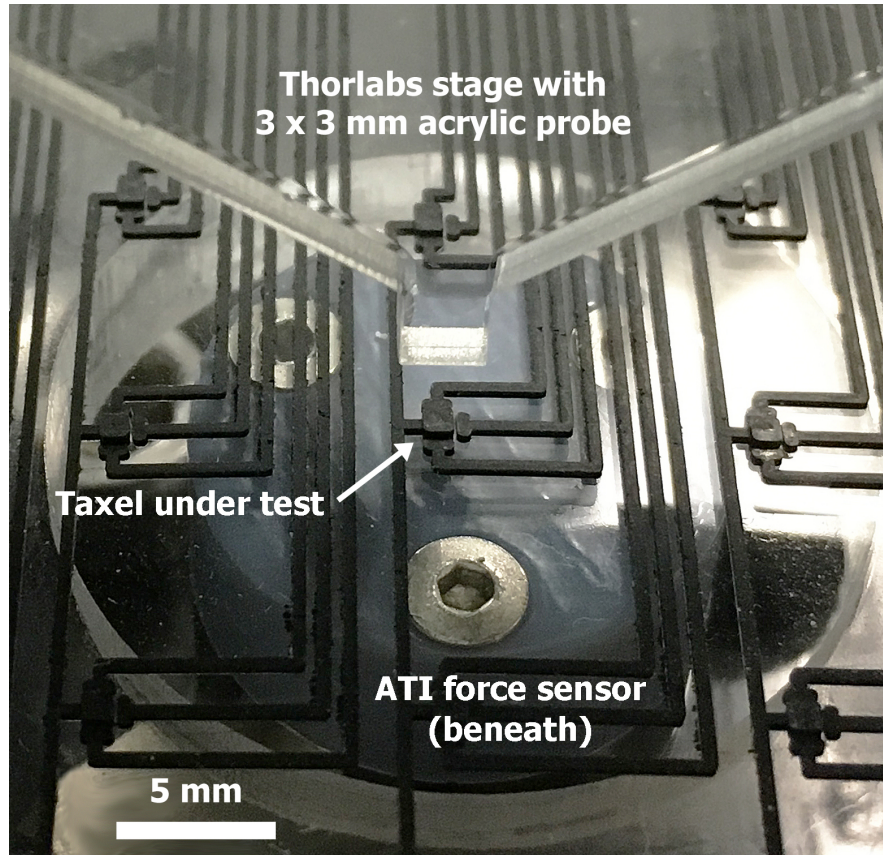


Figure 4: Experimental test setup. A Thorlabs 3-axis stage equipped with an acrylic probe, with a probe tip area of 3 by 3 mm, was used to apply displacements to the robot skin. The resultant forces were read with an ATI Nano17 6-axis force/torque sensor. In the case of contact resistive sensing, an Arduino Uno and voltage divider were used to collect sensor voltages (not pictured). In the case of capacitive sensing, an AD7745/46 evaluation board was used to collect sensor capacitances (not pictured).

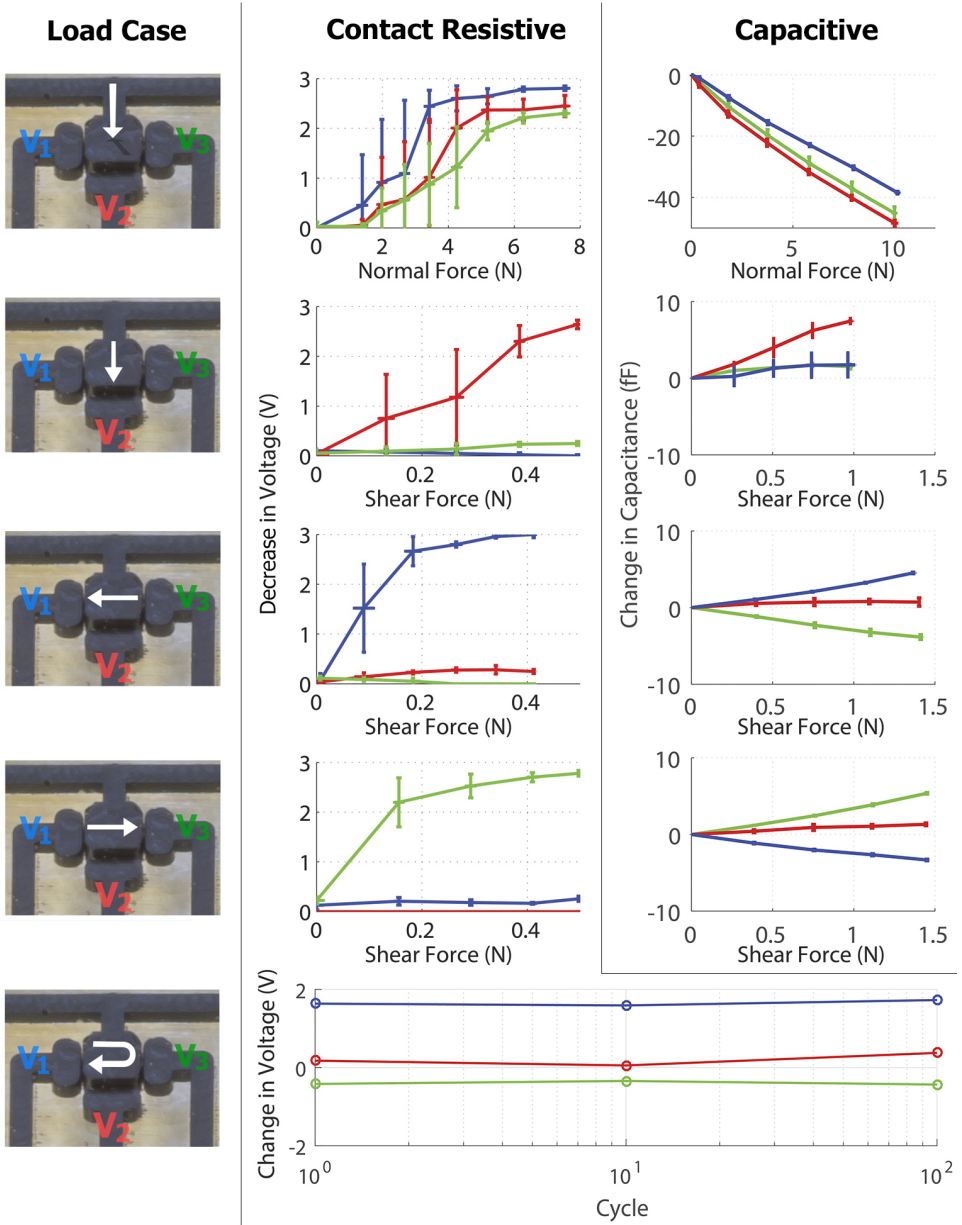


Figure 5: Sensor response to various load cases. Both contact resistive and capacitive transduction methods were characterized, and error bars represent 5 trials of a single taxel. Cyclic shear force testing was also carried out up to 100 cycles for the contact resistive sensor, and no hysteresis was observed.

sensors. Higher shear forces couldn't be tested as the probe was observed to slip. The dynamic range in the normal and shear directions were similar, which was expected due to the FEA guided design that selected a geometry that was a compromise between the two sensing directions. Using the capacitive approach, shear force range and resolution were 1500 mN and 50 mN, respectively. Higher shear forces were possible due to the increased surface area between the PDMS encapsulation and acrylic probe.

## 5.4 Cyclic Loading

Cyclic shear force testing was conducted on a contact resistive taxel by applying a moderate normal force of 4 N followed by loading and unloading of approximately 450 mN of shear force, Fig. 5 [Bottom]. The pad in the direction of loading,  $V_3$ , decreased in voltage while the opposite pad,  $V_1$ , increased in voltage, as intended. The magnitude of the increase in voltage was higher than the decrease due to the pad coming out of contact with pillar. The out-of-plane pad,  $V_2$ , experienced little change in voltage during testing with minor drift near the 100th cycle. No significant hysteresis was observed after 100 cycles.

## 5.5 Spatial Testing

A robot skin the size of an adult human hand was manufactured, and featured 12 contact resistive taxels with a total of 41 electrical leads, Fig. 6. Both normal and shear tests were conducted while the robot skin was resting on a table. In normal testing, each taxel was pressed sequentially by hand, while in shear testing an acrylic plate was slid across the palm area. Snapshots of each test are shown in Fig. 6. In all tests, low noise was seen in taxels not subjected to loading, where changes in voltage were less than 30 mV. In the normal force tests, all 3 pads at each taxel responded with roughly the same magnitude of change in voltage. Meanwhile, in the shear force tests, the pads which were being sheared towards experienced a change in voltage while out-of-plane pads remained relatively unchanged. This demonstrates the ability to achieve 3-axis force sensing over a large area using taxels with microscale features.

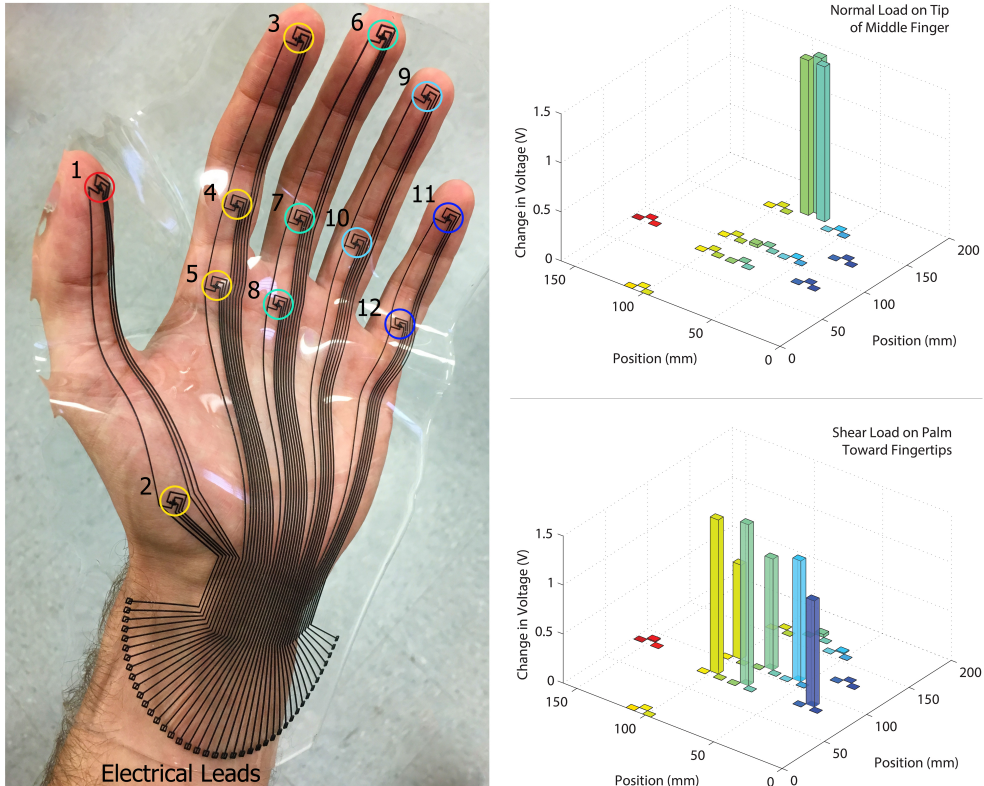


Figure 6: [Left] Robot skin covering an adult hand consisting of 12 contact resistive taxels with a total of 41 electrical leads. Taxels can sense shear and normal forces, and have features as small as  $30 \mu\text{m}$ . [Top Right] Change in voltage of the robot skin when subjected to a normal load applied to the tip of the middle finger (taxel 6). Each pad at the taxel of interest changes in voltage with roughly the same magnitude. [Bottom Right] Change in voltage of the robot skin when subjected to an upward-pointing (toward the fingertips) shear load applied to the palm area (taxels 4, 5, 7, 8, 10, and 12). Pads in the direction of shear loading change in voltage while other pads remain relatively unchanged.

## 6 Closed-Loop Slip Detection

A one degree-of-freedom (DoF) gripper was prototyped to evaluate the robot skin’s performance in a system, Fig. 7 [Top]. A single taxel using the contact resistive approach was mounted onto the tip of a robotic “thumb”. Preliminary tests showed that the gripper was capable of producing a grasp force up to 7-8 N, and was operated around 2-4 N during testing. A closed-loop program was written to: 1) close the thumb until an object was gripped, 2) open the thumb if an object was gripped too tightly, and 3) grip tighter if a high downward-pointing shear force was detected. An Arduino Uno was used for controlling purposes, and the controller was looped through every 250 ms (i.e., 4 Hz sampling rate).

A test was designed to have the gripper grasp an object, and then load the object with a 100 g mass to induce slip. Two cases were tested: without and with slip feedback control, Fig. 7 [Bottom]. In both cases, the 3 pad voltages were nominal (5 V) while the thumb was closing, followed by undulations during thumb-object contact until a soft but stable grasp was reached. When the 100 g mass was applied ( $\sim 1$  N of shear force), in both cases an increase in  $V_1$  and decrease in  $V_3$  was observed, which coincides with a downward-pointing shear force. In the first case, the object was dropped and the pad voltages returned to their nominal value. In the second case, the gripper grasped tighter to prevent dropping the block, and a decrease in the average pad voltage was observed indicating a higher normal force.

## 7 Extensions of Manufacturing Process

The developed milling-based manufacturing process and sensing modality is versatile and adaptable, and can be used to create other elastomer MEMS sensors. For example, the presented 3-axis tactile sensor architecture can be adjusted to accommodate a rat whisker adhered to the pillar, as well as four adjacent pads using a smaller 101  $\mu\text{m}$  endmill (Microcut USA, 82004), Fig. 8. As the whisker is deformed in the shear directions, the pillar and pads come into physical contact resulting in a decrease in voltage. This could enable robots to navigate in the dark [30], or even be repurposed as a flow sensor in which a passing fluid deforms the whisker.

Another example is the creation of a flexible strain sensing skin, such as an artificial moth wing, Fig. 9. Using capacitive sensing, interdigitated

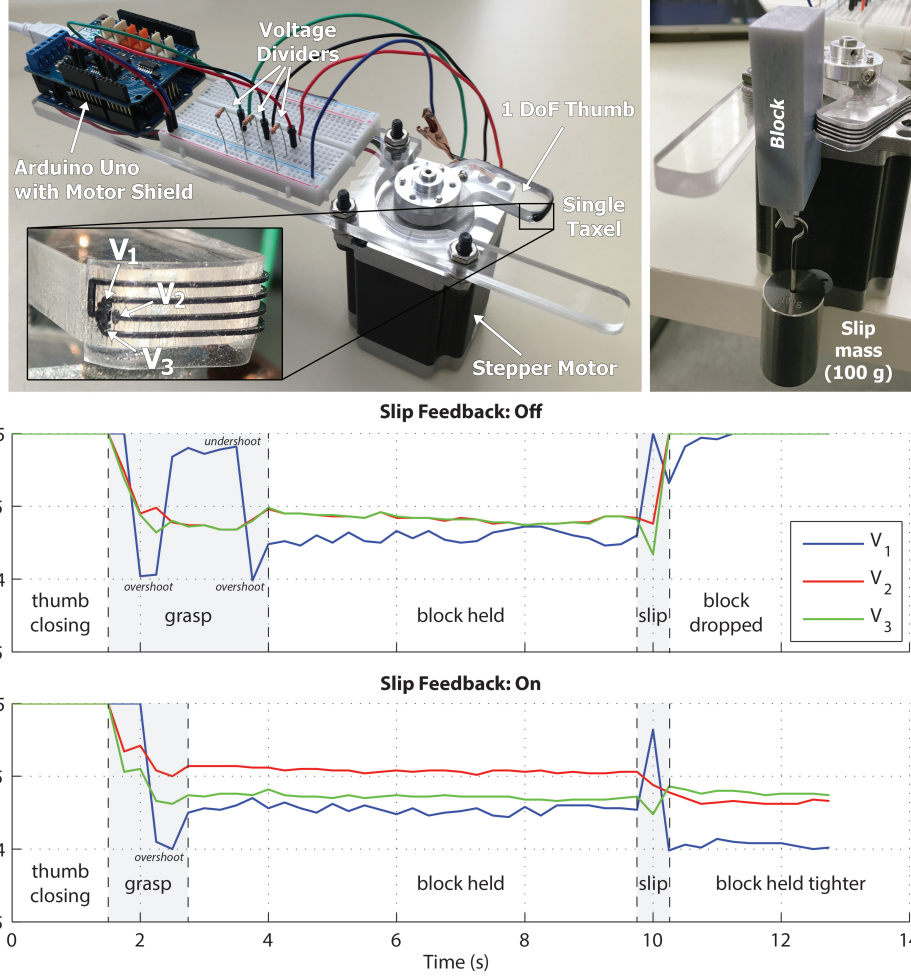


Figure 7: [Top] A one degree-of-freedom gripper equipped with a single contact resistive taxel controlled by an Arduino platform. A mass of 100 g was applied to the block after it was grasped to induce slip. [Bottom] Plots comparing the pad voltages without and with slip feedback control; the difference is evident in the gripper's response after 10 s.

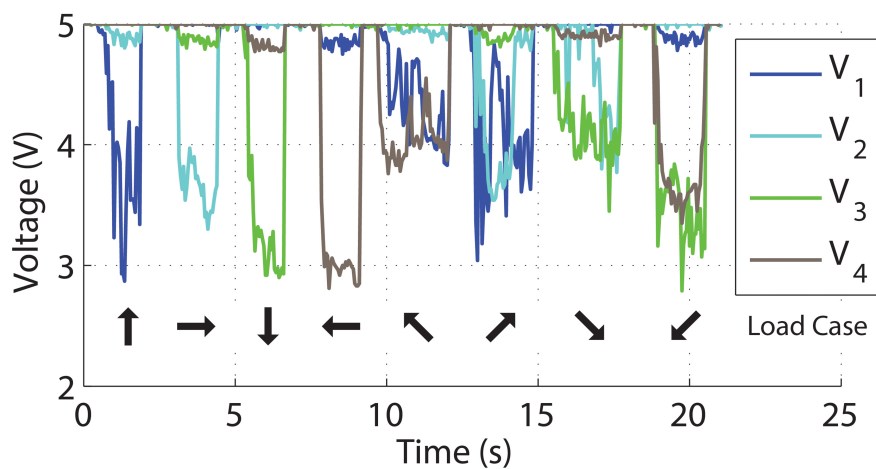
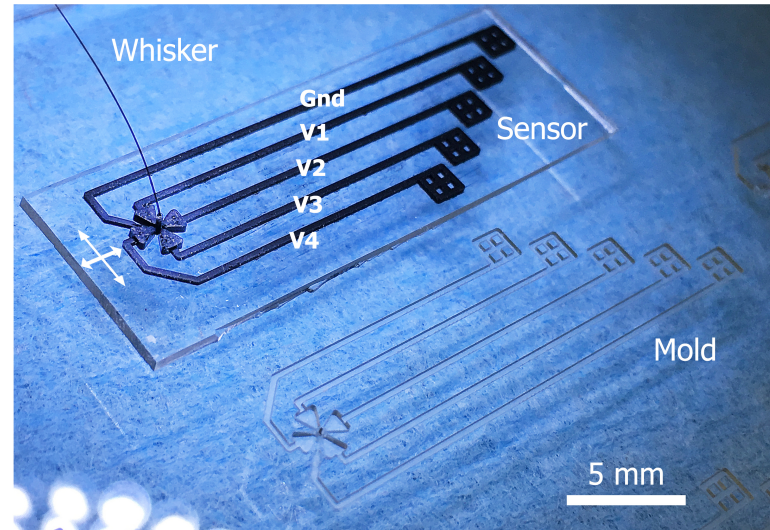


Figure 8: Rat whisker sensor. The taxel design was modified to accommodate 4 pads and a rat whisker press-fit into the center pillar. As the whisker is deflected, the pillar comes into physical contact with the adjacent pads. Eight load cases were tested: 4 cardinal directions and 4 diagonal directions.

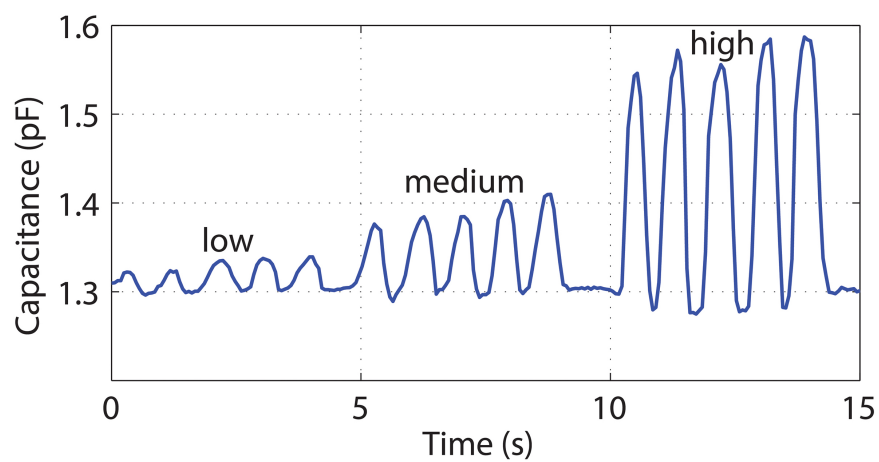
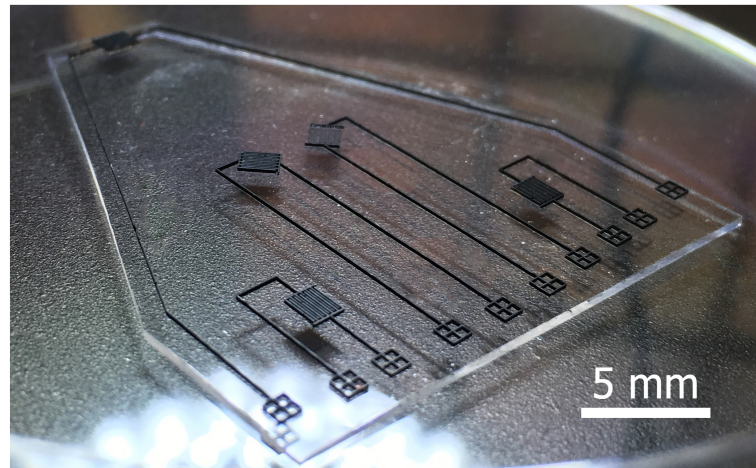


Figure 9: Artificial moth wing outfitted with an array of flexible strain gauges. A capacitive sensing modality was paired with interdigitated electrodes to sense low strains (100s of microstrain) across a wide range.

structures elongate in the direction of strain and cause an increase in capacitance due to the increase in interelectrode area [31]. In this case, a 101  $\mu\text{m}$  in diameter endmill (Microcut USA, 82004) was used to create interdigitated structures with digit widths of 101  $\mu\text{m}$ , depth of 200  $\mu\text{m}$ , and electrode gaps of 90  $\mu\text{m}$ . The mold covered an area of roughly 2 in by 4 in with strain gauges oriented in a fashion similar to other moth wing designs [32]. A single strain gauge on this wing was stretched by hand, and capacitance was collected using the aforementioned AD7745/46 evaluation board. Five cycles were stretched at low, medium, and high strains, where low strain was measured on the order of 100's of microstrain using digital calipers.

## 8 Limitations

Although rapid manufacturing of large area robot skins with 3-axis contact resistive sensing has been demonstrated, the most significant drawback of this particular modality was dynamic range. This can be partly mitigated by tuning the taxel geometry, but still lacks the dynamic range of some previous 3-axis sensors [33, 11]. In the future, dynamic range could potentially be improved by using a rounded contact area rather than flat; this may reduce the deviations between trials. However, capacitive sensing was able to dramatically improve dynamic range; from 8:1 to 100:1 in the normal direction, and from 5:1 to 30:1 in the shear directions. It was also found that at high normal forces (above 8 N), the taxels became relatively insensitive to shear forces as the compressed sensor could not deform further; this is an inherent limitation of the contact resistive approach.

During fabrication, a high amount of force is applied to the acrylic mold as the CNT/PDMS is planarized by hand. During this step, it was found that small gaps tend to break. With a gap of 30  $\mu\text{m}$ , yield was estimated at 80-90%. In the future, larger gaps could be fabricated to improve yield while also increasing the normal force range, or a more delicate planarization process could be employed using liquids like isopropyl alcohol (IPA). A metal instead of acrylic, such as aluminum or steel, could also be used as the stock material to improve gap yield strength.

The contact resistive sensor architecture left the sensing elements exposed to the environment, which could potentially lead to damage from repeated use. Also, conductive objects such as metals were not compatible with this architecture since they created an electrical short between the pillar and

pads. A thin insulating film, such as plastic wrap, can be placed on top of the robot skin to mitigate this.

Electrical routing was fabricated in the same plane as the sensors, limiting the taxel areal density and number of pads per pillar. However, taxel density can increase if a smaller array (ex: 3 by 3 with a spacing of 3 mm, ideal for fingertips) is desired because the amount of routing is significantly less. A smaller diameter endmill for the routing could also be used, as was used in the rat whisker sensor to enable 4 pads per pillar. A more integrated approach would be to mill vias and traces directly into the backside of the robot skin. This step would be done just before peeling the robot skin from the mold (i.e., before the last step in Fig. 3). Then, the vias and traces would be refilled and planarized with CNT/PDMS.

## 9 Conclusion

This work presented a rapid and affordable manufacturing process based on CNC milling, and featured a 3-axis tactile sensor architecture that can use either contact resistance or capacitance to sense forces. The manufacturing process produced features as small as 30  $\mu\text{m}$ , without the need of a clean room, over an area as large as an adult hand. Dynamic range was approximately 8:1 and 5:1 in the shear and normal directions when measuring contact resistance, while capacitive sensing can be used to drastically improve dynamic range up to 100:1. A robot skin was shown to measure shear and normal forces across a large area, and a one DoF gripper was built with a single taxel to demonstrate successful detection and prevention of slip. The ability to quickly manufacture flexible skins will help accelerate the pace of elastomer-based sensor research, and result in new conductive elastomeric sensors.

## Acknowledgment

This work was supported by NASA’s National Robotics Initiative (NRI) grant #NNX12AM02G. The authors would like to thank Anne En-Tzu Yang and Dr. Mitra Hartmann, of Northwestern University, for their assistance in the development of the rat whisker sensor. The authors would also like to thank Will Weston-Dawkes and Hee-Sup Shin for original demonstrations of

the interdigitated strain sensor.

## References

- [1] Hanna Yousef, Mehdi Boukallel, and Kaspar Althoefer. Tactile sensing for dexterous in-hand manipulation in robotics—a review. *Sensors and Actuators A: physical*, 167(2):171–187, 2011.
- [2] Carmel Majidi. Soft robotics: a perspective—current trends and prospects for the future. *Soft Robotics*, 1(1):5–11, 2014.
- [3] Rui Li, Robert Platt, Wenzhen Yuan, Andreas ten Pas, Nathan Roscup, Mandayam A Srinivasan, and Edward Adelson. Localization and manipulation of small parts using gelsight tactile sensing. In *Intelligent Robots and Systems (IROS 2014), 2014 IEEE/RSJ International Conference on*, pages 3988–3993. IEEE, 2014.
- [4] Barrett Heyneman and Mark R Cutkosky. Slip classification for dynamic tactile array sensors. *The International Journal of Robotics Research*, 2015.
- [5] Aaron M Dollar and Hugh Herr. Lower extremity exoskeletons and active orthoses: challenges and state-of-the-art. *Robotics, IEEE Transactions on*, 24(1):144–158, 2008.
- [6] Stacy J Morris and Joseph A Paradiso. Shoe-integrated sensor system for wireless gait analysis and real-time feedback. In *Engineering in Medicine and Biology, 2002. 24th Annual Conference and the Annual Fall Meeting of the Biomedical Engineering Society EMBS/BMES Conference, 2002. Proceedings of the Second Joint*, volume 3, pages 2468–2469. IEEE, 2002.
- [7] Christian Liedtke, Steven AW Fokkenrood, Jasper T Menger, Herman van der Kooij, and Peter H Veltink. Evaluation of instrumented shoes for ambulatory assessment of ground reaction forces. *Gait & posture*, 26(1):39–47, 2007.
- [8] Dustyn P Roberts, Jack Poon, Daniella Patrick, and Joo H Kim. Testing pressurized spacesuit glove torque with an anthropomorphic robotic hand. In *Robotics and Automation (ICRA), 2012 IEEE International Conference on*, pages 1520–1525. IEEE, 2012.

- [9] Sarah Walsh, Daniel Barta, Ryan Stephan, and Stephen Gaddis. Next generation life support (ngls): High performance eva glove (hpeg) technology development element. <http://ntrs.nasa.gov/archive/nasa/casi.ntrs.nasa.gov/20150023265.pdf>, 2015. [Online; accessed 12-May-2016].
- [10] Eric V Eason, Elliot W Hawkes, Marc Windheim, David L Christensen, Thomas Libby, and Mark R Cutkosky. Stress distribution and contact area measurements of a gecko toe using a high-resolution tactile sensor. *Bioinspiration & biomimetics*, 10(1):016013, 2015.
- [11] Alexi Charalambides and Sarah Bergbreiter. A novel all-elastomer mems tactile sensor for high dynamic range shear and normal force sensing. *Journal of Micromechanics and Microengineering*, 25(9):095009, 2015.
- [12] Hyung-Kew Lee, Jaehoon Chung, Sun-Il Chang, and Euisik Yoon. Real-time measurement of the three-axis contact force distribution using a flexible capacitive polymer tactile sensor. *Journal of Micromechanics and Microengineering*, 21(3):035010, 2011.
- [13] Cheng-Wen Ma, Li-Sheng Hsu, Jui-Chang Kuo, and Yao-Joe Yang. A flexible tactile and shear sensing array fabricated using a novel buckypaper patterning technique. *Sensors and Actuators A: Physical*, 231:21–27, 2015.
- [14] Yoshiyuki Ohmura, Yasuo Kuniyoshi, and Akihiko Nagakubo. Conformable and scalable tactile sensor skin for curved surfaces. In *Robotics and Automation, 2006. ICRA 2006. Proceedings 2006 IEEE International Conference on*, pages 1348–1353. IEEE, 2006.
- [15] Vincent Duchaine, Nicolas Lauzier, Mathieu Baril, Marc-Antoine Lacasse, and Clément Gosselin. A flexible robot skin for safe physical human robot interaction. In *Robotics and Automation, 2009. ICRA'09. IEEE International Conference on*, pages 3676–3681. IEEE, 2009.
- [16] Giorgio Cannata, Marco Maggiali, Giorgio Metta, and Giulio Sandini. An embedded artificial skin for humanoid robots. In *Multisensor Fusion and Integration for Intelligent Systems, 2008. MFI 2008. IEEE International Conference on*, pages 434–438. IEEE, 2008.

- [17] Yong-Lae Park, Carmel Majidi, Rebecca Kramer, Phillipre Bérard, and Robert J Wood. Hyperelastic pressure sensing with a liquid-embedded elastomer. *Journal of Micromechanics and Microengineering*, 20(12):125029, 2010.
- [18] Ming-Yuan Cheng, Chun-Liang Lin, Yu-Tse Lai, and Yao-Joe Yang. A polymer-based capacitive sensing array for normal and shear force measurement. *Sensors*, 10(11):10211–10225, 2010.
- [19] Soonjae Pyo, Jae-Ik Lee, Min-Ook Kim, Taeyoung Chung, Yongkeun Oh, Soo-Chul Lim, Joonah Park, and Jongbaeg Kim. Development of a flexible three-axis tactile sensor based on screen-printed carbon nanotube-polymer composite. *Journal of Micromechanics and Microengineering*, 24(7):075012, 2014.
- [20] Letizia Ventrelli, Lucia Beccai, Virgilio Mattoli, Arianna Menciassi, and Paolo Dario. Development of a stretchable skin-like tactile sensor based on polymeric composites. In *Robotics and Biomimetics (ROBIO), 2009 IEEE International Conference on*, pages 123–128. IEEE, 2009.
- [21] Le Cai, Li Song, Pingshan Luan, Qiang Zhang, Nan Zhang, Qingqing Gao, Duan Zhao, Xiao Zhang, Min Tu, Feng Yang, et al. Super-stretchable, transparent carbon nanotube-based capacitive strain sensors for human motion detection. *Scientific reports*, 3, 2013.
- [22] Aaron P Gerratt, Hadrien O Michaud, and Stéphanie P Lacour. Elastomeric electronic skin for prosthetic tactile sensation. *Advanced Functional Materials*, 25(15):2287–2295, 2015.
- [23] Karsten Weiß and Heinz Wörn. The working principle of resistive tactile sensor cells. In *Mechatronics and Automation, 2005 IEEE International Conference*, volume 1, pages 471–476. IEEE, 2005.
- [24] Andreas E Guber, Mathias Hecke, Dirk Herrmann, Alban Muslija, Volker Saile, Lutz Eichhorn, Thomas Gietzelt, Werner Hoffmann, Peter C Hauser, Jatisai Tanyanyiwa, et al. Microfluidic lab-on-a-chip systems based on polymersfabrication and application. *Chemical Engineering Journal*, 101(1):447–453, 2004.

- [25] Kosuke Iwai, Kuan Cheng Shih, Xiao Lin, Thomas A Brubaker, Ryan D Sochol, and Liwei Lin. Finger-powered microfluidic systems using multilayer soft lithography and injection molding processes. *Lab on a Chip*, 14(19):3790–3799, 2014.
- [26] Dario Carugo, Jeong Yu Lee, Anne Pora, Richard J Browning, Lorenzo Capretto, Claudio Nastruzzi, and Eleanor Stride. Facile and cost-effective production of microscale pdms architectures using a combined micromilling-replica moulding ( $\mu$ mi-rem) technique. *Biomedical microdevices*, 18(1):1–10, 2016.
- [27] Paul Day, Eric V Eason, Noe Esparza, David Christensen, and Mark Cutkosky. Microwedge machining for the manufacture of directional dry adhesives. *Journal of Micro and Nano-Manufacturing*, 1(1):011001, 2013.
- [28] Philip N Duncan, Siavash Ahrar, and Elliot E Hui. Scaling of pneumatic digital logic circuits. *Lab on a Chip*, 15(5):1360–1365, 2015.
- [29] Robert D Howe. Tactile sensing and control of robotic manipulation. *Advanced Robotics*, 8(3):245–261, 1993.
- [30] SW Yan, Matthew M Graff, and Mitra JZ Hartmann. Mechanical responses of rat vibrissae to airflow. *Journal of Experimental Biology*, 219(7):937–948, 2016.
- [31] Hee-sup Shin, Alexi Charalambides, Ivan Penskiy, and Sarah Bergbreiter. A soft microfabricated capacitive sensor for high dynamic range strain sensing. In *Intelligent Robots and Systems*. IEEE/RSJ, 2016.
- [32] AL Eberle, BH Dickerson, PG Reinhall, and TL Daniel. A new twist on gyroscopic sensing: body rotations lead to torsion in flapping, flexing insect wings. *Journal of The Royal Society Interface*, 12(104):20141088, 2015.
- [33] Chih-Fan Hu, Wang-Shen Su, and Weileun Fang. Development of patterned carbon nanotubes on a 3d polymer substrate for the flexible tactile sensor application. *Journal of Micromechanics and Microengineering*, 21(11):115012, 2011.